Spin transport in higher *n*-acene molecules

R. Pilevarshahri,[1] I. Rungger,[2] T. Archer,[2] S. Sanvito,[2] and N. Shahtahmassebi[1]
[1]*Physics Department, Faculty of Science, Ferdowsi University of Mashhad, Mashhad, Iran*
[2]*School of Physics and CRANN, Trinity College, Dublin 2, Ireland*
(Received 25 June 2011; revised manuscript received 1 November 2011; published 28 November 2011)

We investigate the spin-transport properties of molecules belonging to the acenes series by using density functional theory combined with the nonequilibrium Green's function approach to electronic transport. While short acenes are found to be nonmagnetic, molecules comprising more than nine acene rings have a spin-polarized ground state. In their gas phase, these have a singlet total spin configuration, where the two unpaired electrons occupy the doubly degenerate highest molecular orbital. Such an orbital degeneracy is however lifted once the molecule is attached asymmetrically to Au electrodes via thiol linkers, leading to a net fractional magnetic moment. In this situation, the system Au/*n*-acene/Au can act as an efficient spin filter with interesting applications in the emerging field of organic spintronics.

DOI: 10.1103/PhysRevB.84.174437 PACS number(s): 75.76.+j, 72.25.Mk, 85.65.+h

I. INTRODUCTION

Molecules of the *n*-acenes family, $C_{4n+2}H_{2n+4}$, are an important class of organic compounds formed from polycyclic aromatic hydrocarbons consisting of linearly fused benzene rings. These molecules, schematically shown in Fig. 1, can be also viewed as small hydrogen-terminated graphene nanoribbons. The interest in their electronic properties has grown enormously in the past few years.[1–24] The smallest acenes, benzene ($n = 1$) and naphthalene ($n = 2$), are well-known aromatic compounds, while the intermediate ones, tetracene ($n = 4$) and pentacene ($n = 5$), are semiconductor materials in their solid phase. These are commonly used in organic field effect transistors,[5,25] organic light emitting diodes,[26,27] and organic photovoltaic cells,[28] because of their high charge carrier mobility. For pentacene single crystals, a value of 35 $cm^2V^{-1}s^{-1}$ was reported,[17] which is among the highest mobilities of all organic semiconductors. As we move to still larger acenes, which we will refer here to as higher acenes, such as heptacene ($n = 7$), octacene ($n = 8$), nonacene ($n = 9$), and decacene ($n = 10$), the structural stability is reduced. Those molecules are in fact quite reactive and the experimental literature becomes less rich. Theoretical studies predict that the higher acenes are good candidates for realizing *p*-type magnetism, i.e., magnetism without ions presenting partially filled *d* or *f* shells.[7–12] If the larger magnetic acenes can be stabilized, their magnetism coupled with the long spin-diffusion length will make this material class extremely appealing for the next generation of organic spintronics devices.[29–33]

The smaller acenes have a nonmagnetic (diamagnetic) ground state. For the higher acenes, calculations predict the edges of the molecule to be spin polarized.[7–9,11,12,18] In this case, there are two degenerate highest occupied molecular orbitals (HOMOs), each of them populated by a single electron. One of the HOMOs is localized mainly on the hydrogenated carbon atoms at one edge of the molecule, while the other HOMO is localized on the opposite edge. These two degenerate molecular orbitals extend in a zigzaglike symmetry along the length of the molecule as indicated by the dashed lines in Fig 1. These states are similar in nature to the edge states found in graphene nanoribbons.[34] The lowest unoccupied molecular orbitals (LUMOs) are the corresponding empty spin-split orbitals, so that the HOMO-LUMO gap is an exchange split gap. Recent calculations predicted a spin-singlet ground state for the higher acenes[7,8,11,12,18] as a result of the antiferromagnetic coupling between the two orbitally degenerate HOMOs, contrary to earlier predictions of a triplet ground state.[10,19,20]

In contrast, in Ref. 13, the molecules are predicted to be nonmagnetic for any length, a fact that is attributed to the axial symmetry of the acene structure. The broken-symmetry solutions obtained with unrestricted spin calculations are found to be higher in energy than the nonmagnetic states. Here, we investigate systems where the axial symmetry is broken explicitly by the asymmetric interaction of the molecules with two electrodes. This lifts the degeneracy between the HOMO levels so that a magnetic solution becomes possible.

Since small acenes are diamagnetic and the higher ones are predicted magnetic, there is a critical length for the onset of magnetism. This is generally accepted to occur for *n* between 6 and 8, but there is no consensus on the precise value. Houk *et al.*[10] used the Becke, 3-parameter, Lee-Yang-Parr (B3LYP) hybrid functional and found that for more than eight acene rings, a triplet ground state is the lowest in energy. Bendikov *et al.*[7,8] performed calculations at the unrestricted B3LYP (UB3LYP) level and observed a magnetic ground state already for six acene rings. Finally, Jiang *et al.*[12] found the transition to a magnetic ground state for more than seven benzene rings.

From the experimental point of view, a significant amount of work has been devoted to the study of electron transport through pentacene.[21–24] The same material has also been used as a medium for spin-polarized transport in composite junctions[35] with some evidence for spin injection.[36] Pentacene itself however is not magnetic. For this reason, significant new effort is being made to synthesize the higher acenes.[1–6,14,16] After much skepticism about its stability,[15] heptacene was finally synthesized in 2006, and subsequent analysis has shown that the ground state is nonmagnetic.[3,16] More recently, Tönshoff and Bettinger synthesized octacene and nonacene,[6] and importantly, they found possible signs for the presence of antiferromagnetism in nonacene.[6]

In this work, we investigate both the ground-state electronic structure and the electronic transport properties of the higher

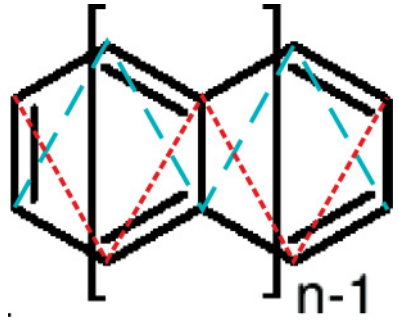

FIG. 1. (Color online) Schematic illustration of the n-acene series. The dashed (light blue) and dotted (red) lines denote the symmetry of the two degenerate HOMOs.

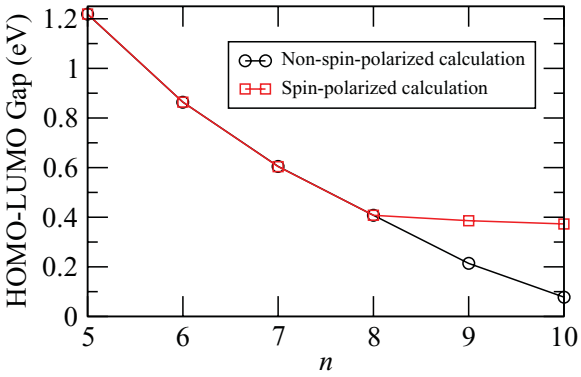

FIG. 2. (Color online) HOMO-LUMO gap calculated from the Kohn-Sham eigenvalues for n-acenes as a function of n.

acenes. In particular, we focus our attention on pentacene and decacene in order to compare results for a nonmagnetic molecule, such as pentacene, to those of a magnetic one, such as decacene.

II. METHODS

The electronic structure is calculated by using spin-polarized density functional theory (DFT), as implemented in the SIESTA code.[37] The transport properties are then obtained with the nonequilibrium Green's function (NEGF) code SMEAGOL,[38–40] which shares the Kohn-Sham Hamiltonian with SIESTA. The local-density approximation (LDA) exchange correlation functional[42] is used throughout this work. A double-ζ (DZ) basis was used to describe the electronic structure of the valence electrons of the molecule, while we use an s-only single-ζ basis set for the gold electrodes. This has been extensively tested in the past[43,44] and offers a good compromise between accuracy and computational demands. A real-space grid with an equivalent plane-wave cutoff of 300 Ry is used to sample the electronic density. For the isolated molecule, periodic images are separated by a minimum of 10 Å, which is found to be sufficient to prevent interaction between the image molecules. For all the molecules, structural relaxation is performed by standard conjugate gradient to a force tolerance of 0.01 eV/Å.

The transport junction is constructed by connecting the molecules to a Au fcc (111) surface via sulfur anchoring groups with a S-Au bond length of 1.9 Å.[41] We use a k-point mesh with a cutoff of 9 Å perpendicular to the transport direction. Due to the presence of many local minima, which are found for the different local magnetic alignments, it was necessary to initialize the calculations with several different spin configurations for both the electronic structure and the transport calculations in order to ascertain the global ground state.

III. RESULTS

We calculate the electronic structure of the isolated n-acenes for the molecules of different lengths ranging from five acene rings ($n = 5$, pentacene) up to ten ($n = 10$, decacene). A nonmagnetic ground state is found for $n \leqslant 8$, whereas nonacene and decacene present a spin-polarized ground state. For these, the atoms at the upper and lower edges of the molecules have an equal and opposite magnetic moment. This is consistent with previous DFT results on higher acenes,[7,12] and it is similar to the edge-state magnetism predicted for graphene nanoribbons.[34] In decacene, the total energy for the antiferromagnetic phase is $\Delta E = 40$ meV smaller than that of the ferromagnetic one and $\Delta E = 110$ meV smaller than that of a non-spin-polarized solution.[12] We note that LDA results for these molecules are in good agreement with those obtained using the B3LYP correlation functional.[7]

We then calculate the HOMO-LUMO gap for all the acenes ranging from pentacene to decacene (see Fig. 2). As the number of benzene rings increases, the HOMO-LUMO gap is reduced. Interestingly, the dependence of the HOMO-LUMO gap on the acene length changes as $n > 8$, i.e., as the molecules develop a spin-polarized ground state. In fact, for the magnetic molecule, the gap is an exchange gap between the spin-split molecular orbitals with the same orbital symmetry. Such an exchange gap is not strongly length dependent and it is expected to saturate to a constant value characteristic of the infinite graphene ribbon. Finally, we note that, if a nonmagnetic solution is forced, one will expect a gap closure for sufficiently long molecules.

It is important to remark at this point that the limitations of the LDA exchange correlation functional make our calculated HOMO-LUMO gap smaller than the experimental one. The experimental gap of pentacene in the gas phase is found to be 5.54 eV,[45] whereas our calculations report a value of only about 1.2 eV. Certainly one should not expect the Kohn-Sham HOMO-LUMO gap to reproduce the true excitation gap of the molecule. Still in the NEGF scheme, the Kohn-Sham eigenvalues are effectively used as single-particle levels for the transport, and one should then ask whether the LDA description is sufficient.[46] Notably, when a molecule is attached to a metallic surface, its ionization potential (IP) is usually reduced due to large correlation effects. In Ref. 47, the HOMO-LUMO gap of pentacene on graphite is calculated by the GW method to be about 2.88 eV. We therefore expect that our LDA HOMO-LUMO gap for pentacene on the surface is underestimated by about a factor of two with respect to experiments. In fact, experimental data[48] return a HOMO-LUMO gap of about 2.2 eV for pentacene thin films on Au. There are no experimental data on the decacene IP, however, we expect a deviation from experiments similar to the one of pentacene.

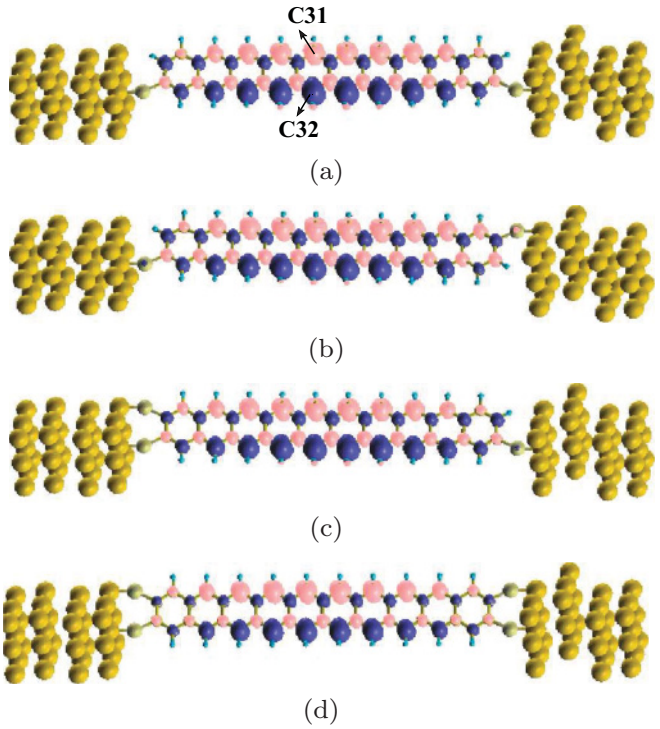

FIG. 3. (Color online) Isosurfaces of spin-density magnetization for the various anchoring geometries of decacene attached to Au via thiol groups: (a) two links, meta, (b) two links, para, (c) three links, and (d) four links. Positive isosurfaces are represented in dark grey (blue) and negative ones in light grey (pink).

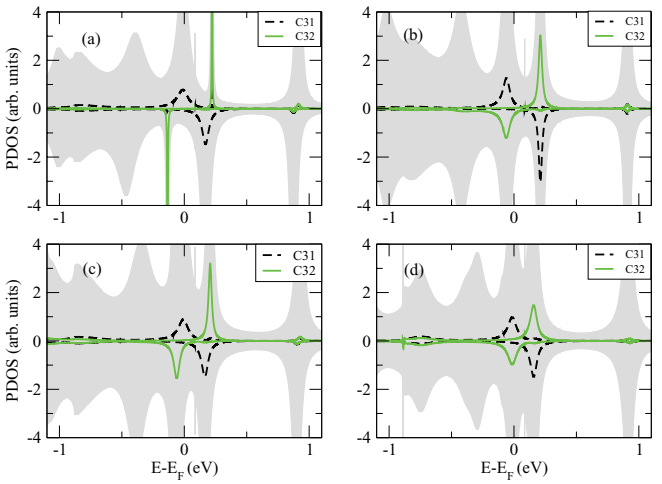

FIG. 4. (Color online) DOS projected on the two carbon atoms in the middle of decacene molecule (C31 and C32) for different anchoring configurations: (a) two links, meta, (b) two links, para, (c) three links, and (d) four links. The grey shadow is the total DOS of the molecule.

We now investigate the electronic structure and the transport properties of the molecules attached to Au electrodes. We use thiol groups to bind the acenes to the Au surface and consider four different binding geometries. These are shown for decacene in Fig. 3. Panel (a) shows the meta configuration, in which only the two ends of the lower edge are connected to Au. Figure 3(b) shows the para configuration, where the lower edge on the left side and the upper edge on the right side are connected to the electrodes. Figure 3(c) corresponds to the meta configuration with an additional S linker on the left side upper edge, and in Fig. 3(d) there are four S linkers.

The ground state of the isolated thiolated molecules is antiferromagnetic for decacene, and nonmagnetic for pentacene. This demonstrates that the electronic structure of the isolated molecules is affected little by the attachment of the S-H end groups. We typically run multiple simulations for each geometry by initializing the density matrix in different spin states. In the case of the complete junction (electrodes plus molecule), we find always an identical final spin configuration regardless of the initialization, so that any other metastable solution cannot be stabilized during the self-consistent cycle. In particular, the calculations for pentacene all converge to a nonmagnetic solution, while those for decacene to a spin-polarized one. In this second case, the coupling to the electrodes determines the final magnetic state.

When the coupling is asymmetric [see Figs. 3(a) and 3(c)] the system develops a significant fractional magnetic moment, while no moment is found for the symmetric geometries [see Figs. 3(b) and 3(d)]. We note that even for asymmetric coupling the direction of the net magnetic moment is arbitrary, however, it might be fixed by an external magnetic field, or by attaching the molecules to ferromagnetic electrodes. In general, the coupling to the electrodes leads to level broadening and consequently to charge transfer from the molecule HOMO to the Au. Thus, whereas the majority HOMO is always fully filled, the minority one may have partial occupation and the total spin polarization may be nonzero. The fact that different density matrix initializations result in the same solution indicates that, at variance with the isolated molecule, which possesses different local energy minima corresponding to different magnetic states, when the molecule is attached to Au there is only one robust global minimum. For the meta configuration, the energy of this single global minimum is about 100 meV smaller than that of the non-spin-polarized solution.

Figure 3 shows the isosurfaces associated to the spin density (the charge density difference between majority and minority spins) of decacene for the four geometries investigated. From the figure, one can notice the general antiferromagnetic coupling between the spins of the two edge states, a characteristic feature of the molecule in its gas phase, which is largely preserved when the molecular junction is made. The coupling to the electrodes in some cases breaks the axial symmetry of the molecule and a magnetic moment arises. This is 0.54 μ_B for the meta configuration [see Fig. 3(a)] and 0.32 μ_B for the structure of Fig. 3(c). No moment is then found for the two symmetric configurations [see Figs. 3(b) and 3(d)].

In order to analyze the effect of the different linking geometries on the electronic structure and on the transport properties of the junctions, we calculate for all the configurations the DOS projected on the two carbon atoms located in the middle of decacene on opposite edges, labeled as C31 and C32 in Fig. 3(a), and the zero-bias transmission coefficient (Figs. 4 and 5). Note that in Fig. 4, we use no additional broadening, so that the width of the DOS peaks is caused entirely by their coupling to the Au electrodes. For the meta configuration [see

Fig. 4(a)], the broadening of the DOS for states located on the upper edge of the molecule (atom C31) is larger than that of the states located on the lower edge (atom C32). This indicates strong coupling for the upper edge state and weak coupling, i.e., stronger localization, for the lower one, as expected from the bonding geometry. The spin splitting of the states with higher coupling to the Au electrodes is reduced from its value for decacene in the gas phase. Furthermore, a strong electron coupling enhances the partial charge transfer from the molecule to the Au electrodes, so that the strongly coupled edge state is closer to the Fermi energy (E_F) for both the HOMO and LUMO. Consequently, the zero-bias transmission [see Fig. 5(a)] for majority and minority spins is different. Intriguingly, at E_F, the transmission coefficient for majority electrons is much larger than that for the minority ones, so that we expect a large spin polarization of the current at small biases. This demonstrates that it is possible to obtain a spin-polarized current in *n*-acenes without using magnetic leads by simply exploiting their intrinsic magnetic nature and by engineering an asymmetric bonding to a metallic surface. These results show that the metal/molecule coupling plays a key role in determining the properties of molecular spintronics devices, in agreement with the results found for nonmagnetic molecules attached to ferromagnetic electrodes.[49–51]

In the para configuration [see Fig. 3(b)], majority and minority states have the same coupling strength to the electrodes, since the two edges of the molecule are identically coupled. The DOS [see Fig. 4(b)] associated to the two edges is symmetric and consequently no spin polarization is seen in the transmission coefficient of Fig. 5(b). Then, when the molecule is anchored to Au through three links [see Fig. 3(c)], although the minority-spin density is not as localized as in the meta configuration, it is still more localized than the majority-spin density. As such also here the electron transmission is different for the two spin directions. Finally, when the molecule is connected to both the edges with a total of four thiol groups, we recover the complete symmetry between the two edges, and

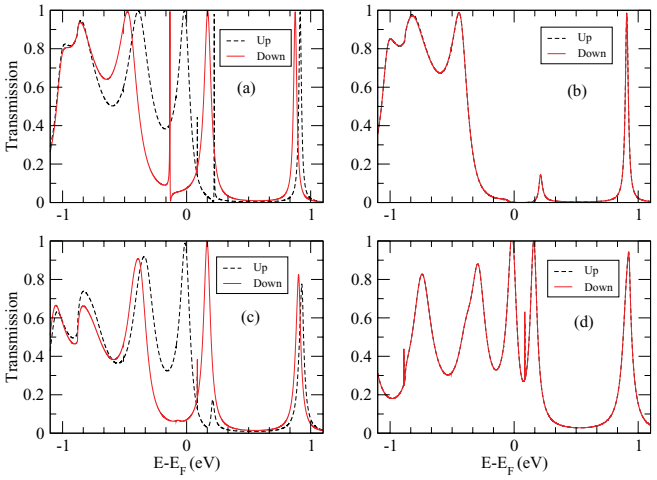

FIG. 5. (Color online) Transmission coefficient for decacene for the different anchoring configurations: (a) two links, meta, (b) two links, para, (c) three links, and (d) four links. "Up" and "Down" indicate the majority- and minority-spin contributions, respectively.

therefore the non-spin-polarized transmission [see Figs. 4(d) and 5(b)].

The coupling strength to the electrodes can be quantitatively described as indicated in Ref. 43. In brief, one can approximate the transmission coefficient as a function of energy, $T_\alpha(E)$, around a particular molecular orbital with energy ϵ_α with a Breit-Wigner-like expression:

$$T_\alpha(E) = \frac{\gamma_\alpha^L \gamma_\alpha^R}{(E-\epsilon_\alpha)^2 + (\gamma_\alpha/2)^2}\,. \qquad (1)$$

Here, γ_α^L (γ_α^R) is the coupling strength of that particular molecular orbital with the left-hand side (right-hand side) electrode. As such the full width at half maximum (FWHM) of a peak in the transmission coefficient is FWHM $= \gamma_\alpha = \gamma_\alpha^L + \gamma_\alpha^R$. For symmetric coupling to the electrodes, we have $\gamma_\alpha^L = \gamma_\alpha^R =$ FWHM/2. Note that the same level broadening is found for the DOS and that this can be directly extracted from the NEGF density matrix.

Let us focus as an example on the meta configuration. In this case, the majority-spin levels, localized on the upper edge of the molecule, are coupled to the electrodes via the thiol group. In contrast, the minority-spin levels, localized on the lower edge, can be accessed from the electrodes only through tunneling in vacuum, since there is no direct binding atom. We then calculate a FWHM for the majority HOMO and LUMO of 100 and 67 meV, respectively. Although minor differences in the orbital wave function produce differences in the FWHM, we conclude that the overall coupling of the upper edge levels is of the order of $\gamma_\alpha = 84$ meV, which corresponds to a lifetime of 5 ps. The same analysis carried out for the minority spins gives us $\gamma_\alpha = 2$ meV and a lifetime of 200 ps. We then conclude that the electronic coupling of the thiolated edge is approximately 40 times stronger than that of the nonthiolated one.

We now briefly discuss the potential consequences arising from the LDA underestimation of the HOMO-LUMO gap. In general, the main drawback is that both the HOMO and the LUMO are artificially too close to the electrodes E_F. Therefore the calculated charge transfer from the molecule majority HOMO to Au (about 0.13 electrons in this case) is likely to be overestimated. As a consequence, also the net magnetic moment is probably overestimated. If one assumes that the charge transfer is negligible at zero bias then the total magnetic moment will be close to zero. However, even in such

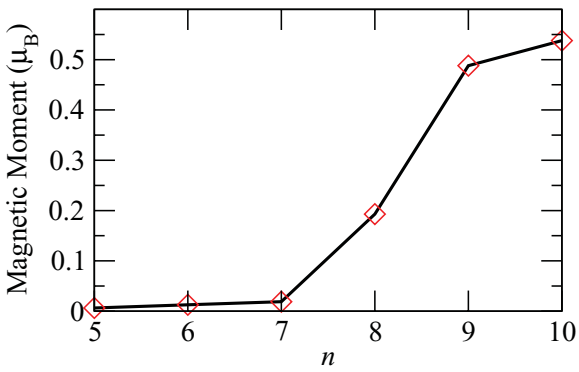

FIG. 6. (Color online) Magnetic moment of the Au/*n*-acene/Au junction as a function of the molecule length, *n*.

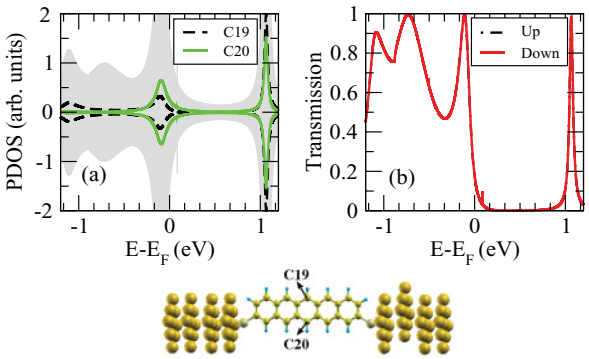

FIG. 7. (Color online) (a) DOS projected on the two carbon atoms in the middle of the pentacene molecule (C19 and C20) and (b) transmission coefficient for pentacene attached to Au in meta anchoring configuration. The grey shadow is the total DOS of the molecule.

a situation, a charge transfer and consequently a net magnetic moment can originate either at finite bias or by applying an electrostatic gate to the molecules. Therefore the finding of a total magnetic moment on the molecule is a general feature of such an interface, since it depends entirely on the fact that there is a considerably different electronic coupling to Au for the two spin channels of the molecule. The fact that such a magnetic moment can be potentially tuned via bias or gate voltage opens intriguing possibilities for device applications.

In order to compare results for molecules of different length, we performed additional calculations for the Au/n-acene/Au junction in the meta configuration and for different n. In general, we find spin-polarized transmission for molecules made up of more than eight rings (see Fig. 6 for the magnetic moment of the junction as a function of n). The features of these magnetic molecule junctions are qualitatively similar to those described in details for decacene. We have also performed calculations within the generalized gradient approximation (GGA) for the exchange correlation functional.[52] The GGA results agree with the LDA ones, except for the fact that when using GGA, the transition from the unpolarized to the spin-polarized solution occurs at $n = 7$ for the isolated molecule and at $n = 6$ for the molecule attached in meta configuration to Au.

For the sake of comparison, in Fig. 7, we present the DOS and the zero-bias transmission for a representative nonmagnetic acene, namely, pentacene. Since the ground state is nonmagnetic, the DOS of the carbon atoms on the upper edge is the same as that on the lower edge. This is illustrated in Fig. 7 by plotting the DOS projected on the central C atoms on upper (C19) and lower (C20) edges. Therefore we find a completely non-spin-polarized zero-bias transmission [see Fig. 7(b)]. Importantly, transport measurements for pentacene on Au indicate hole conductance.[17] This is consistent with our results, which do indicate HOMO transport. However, due to the underestimated IP, our low-bias conductance is likely to be overestimated.

IV. CONCLUSIONS

We have examined the electronic structure and spin transport properties of higher acenes molecules attached to Au electrodes. These have been compared with those of the smaller members of the acene family. We find that the isolated molecules have a spin-polarized ground state for molecules containing more than eight acene rings, however, the net magnetic moment vanishes. When such molecules are attached to Au via thiol linkers, a transition from a nonmagnetic to a magnetic ground state occurs at eight acene rings. The coupling between the two HOMO levels is still found to be antiferromagnetic. However, when the electronic interaction of the molecule with the electrodes is different between the two molecule edges then fractional charge transfer leads to a total net spin. The Au/n-acene/Au system acts then as a spin filter. Such a spin-filtering property can be achieved by binding the molecule to Au via thiol linkers in an asymmetric way. We finally speculate on the fact that the charging state of the molecule and hence its magnetic moment can be controlled by bias and/or electrostatic gating.

ACKNOWLEDGMENTS

I.R., T.A., and S.S. acknowledge financial support from Science foundation of Ireland (07/IN.1/I945 and No. 07/RFP/PHYF235), CRANN, and the EU FP7 project ATHENA and R.P. and N.S. from Iran Ministry of Science, Research and Technology. Computational resources have been provided by the HEA IITAC project managed by TCHPC and by ICHEC.

[1] D. Chun, Y. Cheng, and F. Wudl, Angew. Chem. **120**, 8508 (2008).
[2] I. Kaur, M. Jazdzyk, N. N. Stein, P. Prusevich, and G. P. Miller, J. Am. Chem. Soc. **132**, 1261 (2010).
[3] R. Mondal, B. K. Shah, and D. C. Neckers, J. Am. Chem. Soc. **128**, 9612 (2006).
[4] M. M. Payne, S. R. Parkin, and J. E. Anthony, J. Am. Chem. Soc. **127**, 8028 (2005).
[5] J. Anthony, Angew. Chem. Int. Ed. **47**, 452 (2008).
[6] C. Tönshoff and H. F. Bettinger, Angew. Chem. Int. Ed. **49**, 4125 (2010).
[7] J. M. Bendikov, H. M. Duong, K. Starkey, K. N. Houk, E. A. Carter, and F. Wudl, J. Am. Chem. Soc. **126**, 7416 (2004).
[8] J. M. Bendikov, H. M. Duong, K. Starkey, K. N. Houk, E. A. Carter, and F. Wudl, J. Am. Chem. Soc. **126**, 10493 (2004).
[9] M. C. dos Santos, Phys. Rev. B **74**, 045426 (2006).
[10] K. N. Houk, P. S. Lee, and M. Nendel, J. Org. Chem. **66**, 5107 (2001).
[11] J. Hachmann, J. J. Dorando, M. Aviles, and G. K. Chan, J. Chem. Phys. **127**, 134309 (2007).
[12] D. Jiang and S. Dai, J. Phys. Chem. A **112**, 332 (2008).

[13]B. Hajgató, D. Szieberth, P. Geerlings, F. D. Proft, and M. S. Deleuze, J. Chem. Phys. **131**, 224321 (2009).
[14]Sanjio S. Zade and M. Bendikov, Angew. Chem. Int. Ed. **49**, 4012 (2010).
[15]E. Clar, *Polycyclic Hydrocarbons* (Academic Press, London, 1964), Vol. 1.
[16]H. F. Bettinger, R. Mondal, and D. C. Neckers, Chem. Commun., 5209 (2007).
[17]O. D. Jurchescu, J. Baas, and T. T. M. Palstra, Appl. Phys. Lett. **84**, 3061 (2004).
[18]Z. Qu, D. Zhang, C. Liu, and Y. Jiang, J. Phys. Chem. A **113**, 7909 (2009).
[19]H. Angliker, E. Rommel, and J. Wirz, Chem. Phys. Lett. **87**, 208 (1982).
[20]N. Nijegorodov, V. Ramachandran, and D. P. Winkoun, Spectrochim. Acta, Part A **53**, 1813 (1997).
[21]J. Puigdollers, C. Voz, I. Martin, A. Orpella, M. Vetter, and R. Alcubilla, J. Non-Cryst. Solids **338-340**, 617 (2004).
[22]H. Yanagisawa, T. Tamaki, M. Nakamura, and K. Kudo, Thin Solid Films **464-465**, 398 (2004).
[23]A. El Amrani, B. Lucas, and A. Moliton, Eur. Phys. J. Appl. Phys. **41**, 19 (2008).
[24]L. Diao, C. D. Frisbiea, D. D. Schroepfer, and P. P. Ruden, J. Appl. Phys. **101**, 014510 (2007).
[25]S. K. Park, T. N. Jackson, J. E. Antony, and D. A. Mourey, Appl. Phys. Lett. **91**, 063514 (2007).
[26]B. B. Jang, S. H. Lee, and Z. H. Kafafi, Chem. Mater. **18**, 449 (2006).
[27]M. A. Wolak, B. B. Jang, L. C. Palilis, and Z. H. Kafafi, J. Phys. Chem. B **108**, 5492 (2004).
[28]B. P. Rand, J. Genoe, P. Heremans, and J. SPoortmans, J. Prog. Photovoltaics **15**, 659 (2007).
[29]S. Sanvito, J. Mater. Chem. **17**, 4455 (2007).
[30]S. Sanvito, Nat. Mater. **6**, 803 (2007).
[31]V. A. Dediu, L. E. Hueso, I. Bergenti, and C. Taliani, Nat. Mater. **8**, 707 (2009).
[32]L. Bogani and W. Wernsdorfer, Nat. Mater. **7**, 179 (2008).
[33]G. Szulczewski, S. Sanvito, and J. M. D. Coey, Nat. Mater. **8**, 693 (2009).
[34]X. H. Zheng, I. Rungger, Z. Zeng, and S. Sanvito, Phys. Rev. B **80**, 235426 (2009).
[35]T. Shimada, H. Nogawa, T. Noguchi, Y. Furubayashi, Y. Yamamoto, Y. Hirose, T. Hitosugi, and T. Hasegawa, Jpn. J. Appl. Phys. **47**, 1184 (2008).
[36]T. Ikegami, I. Kawayama, M. Tonouchi, S. Nakao, Y. Yamashita, and H. Tada, Appl. Phys. Lett. **92**, 153304 (2008).
[37]J. M. Soler, E. Artacho, J. D. Gale, A. Garcia, J. Junquera, P. Ordejón, and D. Sanchez-Portal, J. Phys. Condens. Matter **14**, 2745 (2002).
[38]A. R. Rocha, V. M. Garcia-Suarez, S. W. Bailey, C. J. Lambert, J. Ferrer, and S. Sanvito, Nat. Mater. **4**, 335 (2005).
[39]A. R. Rocha, V. M. Garcia-Suarez, S. W. Bailey, C. J. Lambert, J. Ferrer, and S. Sanvito, Phys. Rev. B **73**, 085414 (2006).
[40]I. Rungger and S. Sanvito, Phys. Rev. B **78**, 035407 (2008).
[41]C. Toher, I. Rungger, and S. Sanvito, Phys. Rev. B **79**, 205427 (2009).
[42]J. P. Perdew and A. Zunger, Phys. Rev. B **23**, 5048 (1981).
[43]C. D. Pemmaraju, I. Rungger, and S. Sanvito, Phys. Rev. B **80**, 104422 (2009).
[44]I. Rungger, X. Chen, U. Schwingenschlögl, and S. Sanvito, Phys. Rev. B **81**, 235407 (2010).
[45]M. Yu. Dolomatov and G. R. Mukaeva, J. Appl. Spectrosc. **53**, 1286 (1991).
[46]C. Toher, A. Filippetti, S. Sanvito, and K. Burke, Phys. Rev. Lett. **95**, 146402 (2005).
[47]J. B. Neaton, M. S. Hybertsen, and S. G. Louie, Phys. Rev. Lett. **97**, 216405 (2006).
[48]N. Koch, A. Kahn, J. Ghijsen, J.-J. Pireaux, J. Schwartz, R. L. Johnson, and A. Elschner, Appl. Phys. Lett. **82**, 70 (2003).
[49]S. Sanvito, Chem. Soc. Rev. **40**, 3336 (2011).
[50]C. Barraud, P. Seneor, R. Mattana, S. Fusil, K. Bouzehouane, C. Deranlot, P. Graziosi, L. Hueso, I. Bergenti, V. Dediu, F. Petroff, and A. Fert, Nat. Phys. **6**, 615 (2010).
[51]S. Sanvito, Nat. Phys. **6**, 562 (2010).
[52]J. P. Perdew, K. Burke, and M. Ernzerhof, Phys. Rev. Lett. **77**, 3865 (1996).